Effect of Thermal Aging on Impact Toughness of Electron Beam-Welded AISI 316 Stainless Steel

Arun Kumar, Sandeep Singh Sandhu and Beant Singh

Abstract Thick section of cold-rolled austenite stainless steel AISI 316 is widely used in heat exchangers, jet engines, furnace parts, exhaust manifolds, fast breeder test rector, etc., because of its high strength, corrosion, and pitting resistance properties at high working temperature 400–550 °C approximately. Electron beam welding is considered as highly efficient welding process in order to achieve high-quality welds with low heat-affected zone. In this paper, single-pass narrow gap square butt welding of 18-mm-thick plates using electron beam welding at constant accelerating voltage 150 kV, beam current 90 mA, welding travel speed 600 mm/min, and beam oscillation in circular pattern was investigated. The impact toughness and metallurgical properties in as-welded condition and after imparting post-weld thermal aging (PWTA) at 750 °C for 24 h were also investigated in this piece of work. The full penetration had been achieved in single pass by optimizing the relationship between welding parameters (beam accelerating voltage, beam current, welding travel speed, and beam oscillation). The results showed that welding of plates without filler metal leads to defect-free welds. The average impact toughness conducted by Charpy impact test at cryogenic temperature (−40 °C) in as-welded samples was recorded as 284 J, and after aged at 750 °C for 24 h it reduced to 180 J.

Keywords AISI 316 SS · Electron beam welding · Microstructure · Microhardness · Cryogenic impact toughness

A. Kumar · S. S. Sandhu (✉)
Department of Mechanical Engineering, Quest Infosys Foundation Group of Institutions, Jhanjeri, Mohali, Punjab 140307, India
e-mail: ersandeepsandhu@gmail.com

A. Kumar
e-mail: arunjaito@gmail.com.com

B. Singh
Department of Mechanical Engineering, Punjab College of Engineering and Technology, Lalru, Punjab, India
e-mail: beantsingh7@yahoo.co.in

J. Li et al. (eds.), *Characterization of Minerals, Metals, and Materials 2020*,
The Minerals, Metals & Materials Series,
https://doi.org/10.1007/978-3-030-36628-5_16

Introduction

AISI 316 austenitic stainless steel (SS) is widely used in nuclear power plants, heat exchangers, and fast breeder test reactors [1] as structural materials. The preference of this alloy is due to its high-temperature tensile strength, fatigue strength along with excellent fracture toughness in combination with excellent weldability and fabricability. The joining of 316-type austenitic stainless steel by welding processes and its exposure to harsh environment can be the cause of the formation of various phases which can affect its properties significantly. Raghunathan et al. [2] reported that AISI 316 SS when heat-treated between the temperature range of 900 and 1100 °C, the ferrite content of the weld decreases with increase in aging time. Moreover, the dendritic morphology of ferrite phase tried to break up and spheroidize. Kar et al. [3] investigated that electron beam (EB)-welded joints possessed similar tensile properties at room temperature and at 700 °C irrespective of being prepared with beam oscillation or non-oscillating beam. Dutt et al. [4] concluded that resistance to crack initiation of 316(N) welds decreased when aged at 370, 475, and 550 °C for 20,000 h. The Charpy energy values decreased when aged at 475 °C for 20,000 h. The embrittlement of the welds occurred at 370–550 °C for long durations leads to decline in mechanical properties.

Xia et al. [5] concluded that beam oscillation in electron beam welding leads to uniform weld morphology and increased the weld width. The ferrite morphology changed from lathy/skeletal grains in the top layer to equiaxed grains at bottom of the bead. Further, they also claimed that the solidification of fusion zone (FZ) changed due to beam oscillation. However, beam oscillation had a very little impact on microstructure. Alali et al. [6] concluded that finer dendritic structure was noticed at the bottom of the weld zone. The weld centerline contained a microstructural boundary is called parting. The yield strength of bottom section of the weld metal was 14–52 MPa higher than top section. The tensile testing specimens extracted from the bottom of the weld had 4% higher UTS than the specimens extracted from top of the weld. The entire lot of tensile specimen failed at the center of the fusion zone usually at the parting region.

Zumelzu et al. [7] concluded that the thermal contribution was directly proportional to the ferrite content and tensile strength in 316 L SS weld joints. Joseph et al. [8] varied the electron beam power from 3 to 4.2 kW while welding and concluded that by increasing Q/V ratio the hardness and toughness of the material decreased which is due to the variation in the cooling rate. Kim et al. [9] concluded that heat-treating 316 SS at 600 °C for 10 h resulted in a very little change in the microstructure. The heat treatment for 650 and 700 °C reduced the mechanical properties. Further, when HAZ of 316 was heat-treated for 600 °C for 10 h the tensile strength reduces marginally but was still higher than base metal. Kozuh et al. [10] concluded that tensile strength of the weld metal was higher than the parent metal and the impact toughness decreased with increase in annealing temperature. Further, post-weld heat treatment decreased the value of microhardness for both the base and HAZ. The increase in annealing temperature led to decrease in delta ferrite

content. Xia et al. [11] after conducting the microstructure analysis concluded that weld metal was composed of austenitic matrix along with dendritic ferrite. As the thickness increased, the morphology of delta ferrite changed to columnar equiaxed ferrite from skeletal, lacy, and lathy ferrite. The fusion zone had lower hardness as compared to base metal due to the presence of coarse columnar grains and increasing delta ferrite content. Balaji et al. [12] concluded that thermal aging has an adverse affect on the mechanical properties of 316 steel as it gets embrittled. Embrittlement is mainly due to precipitation of $M_{23}C_6$ carbides on the grain boundaries.

Kar et al. [13] stated that electron beam oscillation resulted in better mechanical properties as compared to non-beam oscillation. Due to the higher cooling rate, the width of fusion zone in beam oscillation EB welds was less than non-beam oscillating EB welds. The microstructure revealed that EB welds contain similar content of δ ferrite with skeletal and lathy morphology with non-beam oscillation and beam oscillation, respectively. Tjong et al. [14] investigated that the microstructure study showed that high cooling and under-cooling associated with electron beam and laser welding caused formation of cellular and equiaxed dendrites in both EB and laser welds. The hardness in both the cases was higher in HAZ and weld metals than the base metal.

Shaikh et al. [15] concluded that aging of 316 L SS weld metal at 600 °C for 20 h resulted in precipitations of carbides. On the contrary when aged at 20,000 h resulted in the formation of sigma phase. They also found that matrix softening had a significant effect on yield strength whereas UTS was influenced by matrix hardening.

Chen and Gan [16] observed that the formation of carbides in the grain boundaries caused cracking and shearing which destabilized the grain boundaries. These alterations in grain boundaries reduced the ductility leading to the reduction in tensile elongation and also reduced the impact strength of the material. Further, they concluded that the reduction in impact strength mainly depended on the ageing time. The carbides were fine and denser in the specimens thermally aged at 650 and 750 °C with normal aging time and at 550 °C after long aging time and lead to the high reduction in tensile elongation and impact strength. High-temperature thermally aged specimens (900 °C) had large size carbides at the grain boundaries causing reduction in elongation. The present work aimed at fabrication of completely penetrated electron beam welds of 18-mm thick AISI 316 SS plates, confirming to sound industrial quality. Further, the welds were examined for impact toughness and metallurgical properties in the as-welded state and after aging at 750 °C for 24 h, in order to study the effect of precipitating phase on the performance of AISI 315 SS welds.

Experimental Procedure

In this study, the rolled and annealed AISI 316 austenitic stainless steel workpieces of 400 mm × 75 mm × 18 mm were used. The length was transverse to rolling direction. The chemical composition obtained by spectroscopic analysis is shown in Table 1.

Table 1 Chemical composition of the base material AISI 316 SS (wt%)

Element	C	Si	Mn	S	P	Cr	Ni	Mo	Cu	Ti	V	Co	Nb	W	Fe
AISI 316	0.064	0.538	0.948	0.025	0.023	16.146	10.441	2.178	0.191	0.009	0.061	0.025	0.041	0.007	Balance

Table 2 Welding parameters employed in the present work

Beam voltage, V (kV)	Beam current, I (mA)	Welding speed (mm/min), S	Oscillation pattern	Oscillation frequency	Heat input (KJ/mm)
150	90	600	Circle	800 Hz	1.28

Heat input per unit length of weld $= \eta\ (V \times I)/S.$, whereas η denotes heat source efficiency (taken as 0.95), V is beam voltage, I is beam current, and S is beam travel speed

Electron beam welding (EBW) in autogenous mode, i.e. welding without filler metal, was used to achieve single-pass, full penetration square butt joint. Before welding, edges of the plates were carefully machined by using milling machine to obtain perfect square and were cleaned by acetone to remove dust, rust, etc. The vacuum pressure in the working chamber of EBW machine was approximately 5×10^{-6} mbar, and the gun pressure was approximately 2×10^{-6} mbar. The welding parameters used in this study are shown in Table 2.

The metallographic specimens were cut precisely by wire-cut EDM for microstructure analysis by using optical microscope. To reveal the microstructure, the specimens were polished using emery paper of 80–3000 grit size and the specimens were chemically etched by aqua regia solution (1 part of HNO_3 and 3 parts of HCl) for 15–20 s. The specimens prepared were thermally aged at 750 °C for 24 h followed by air cooling to facilitate the precipitation of the carbides. The microhardness values (approximately 5 readings per point) were taken across (from left to right with a spacing of 0.15 mm) and along the weld bead centerline (from top to bottom with 0.5 mm spacing) as indicated in Fig. 1. Vickers microhardness testing of weld bead was carried using a load of 1 kg for a dwell time of 20 s. The Charpy V-notch impact test specimens from welded joint were cut according to the ASTM E23 standard from three locations (top, middle, and bottom). Charpy impact tests were carried out at cryogenic temperature (−40 °C) on specimens of 55 mm × 10 mm × 6 mm dimensions. To measure the error in readings, three specimens were tested from one location.

Results and Discussion

Morphology of the Welds

The cross-sectional view of the weld joint fabricated using EBW process is shown in Fig. 1. The macrostructure shows the regions of base metal, HAZ and FZ. The through weld was obtained along 18 mm thickness of the weld plates, and it penetrated 1/4 of the backing plate. The macrostructure shows dagger-shaped weld bead (wide top and narrow bottom regions) obtained without any weld defects. The total welding heat input per unit length was 1.28 kJ/mm. During the EBW, the molten metal deposits

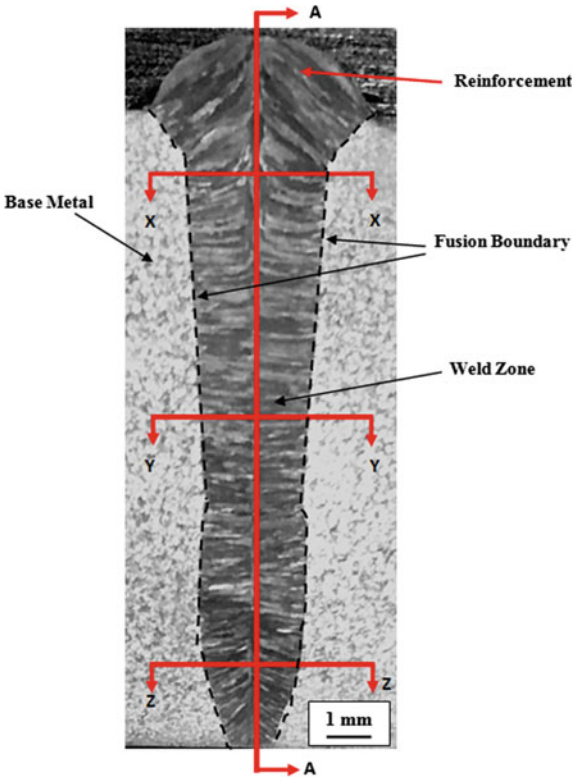

Fig. 1 Macrostructure of EB welds; *X–X-*, *Y–Y-*, and *Z–Z-*axes represent the location across the weld centerline, and *A–A* represents along the weld centerline

at the top side (keyhole mode welding), and the total heat accumulation was more on the top of the weld due to large weld volume accumulation which further leads to slower cooling rates and vice versa on the middle and bottom weld bead. The optical microstructures of the welds in the as-welded and after post-weld thermal aging treatment (750 °C for 24 h) are shown in Figs. 2 and 3 respectively. The weld microstructure consists of austenite matrix along with dendritic δ ferrite grains. The EBW increases the cooling rate of the molten metal which results in non-uniform solidification, hence incomplete ferrite to austenite transformation [17]. Figure 2b depicts the microstructure of the fusion zone at the top of the weld bead, which shows the presence of columnar grains growing perpendicular to the parting line. The vermicular structure of ferrite dendrites was visible within the parting line.

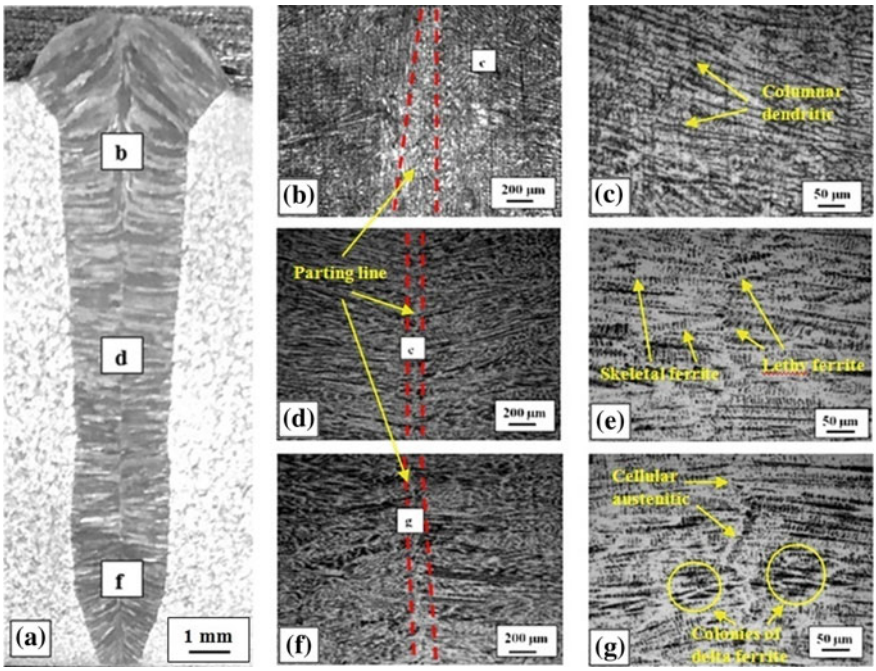

Fig. 2 Macrostructure and microstructure of EB as-welded joint. **a** Macrostructure of FZ, **b** columnar structure at top part of weld bead at 50×, **c** top part of weld bead at higher magnification, 200×, **d** columnar and equiaxed delta ferrite at middle of weld bead, 50×, **e** lathy structure at middle of weld bead, 200×, **f** delta ferrite formation at bottom of the FZ, 50×, **g** primary austenitic structure at bottom of the FZ, 200×

Figure 2c shows higher magnification of columnar grains growing towards the parting line. Figure 2d depicts the microstructure of the middle zone of the weld bead. The microstructure in this area consists of both equiaxed and columnar delta ferrites, and this may be due to higher cooling rates at the center than the top of the weld bead. Figure 2e shows the magnified view of the grains at the centerline, which shows the formation of lathy ferrite at the weld centerline and skeletal ferrite at weld zone. Figure 2f shows microstructure of fusion zone at the bottom of the weld. The microstructure consists of colonies of delta ferrite forming from the parting line, growing outwards. The weld centerline had cellular austenitic structure, which could be due to higher cooling rates at the bottom of the weld bead [18, 19].

Figure 3 shows the macrostructure and microstructure of weld bead after PWTA (750 °C for 24 h). After aging, the microstructures at top, middle, and bottom show the precipitation of carbides in the austenitic network.

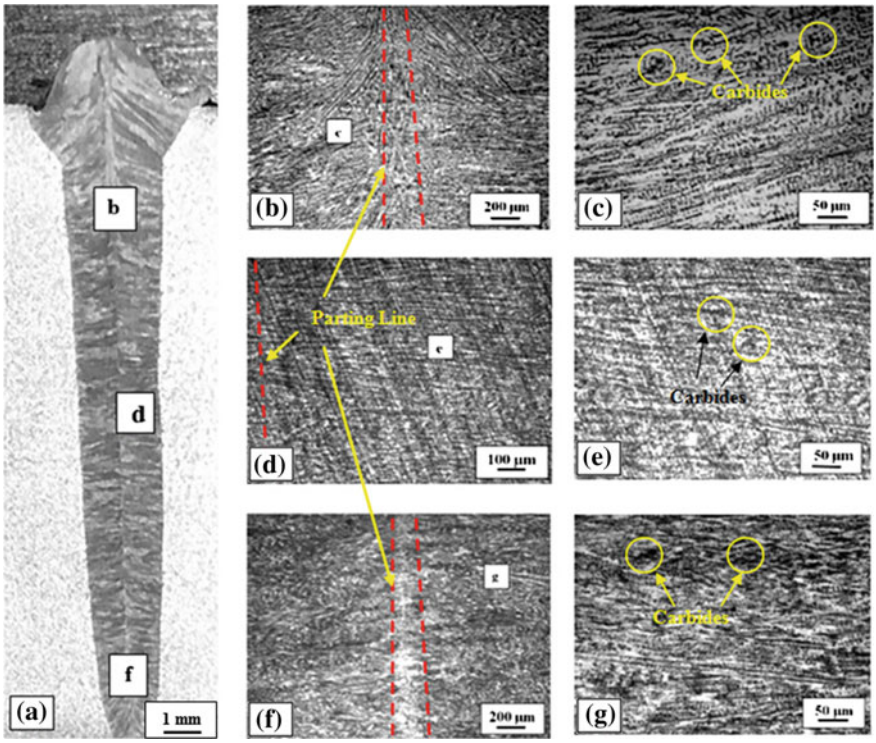

Fig. 3 Macrostructure and microstructure of PWTA specimen. **a** Macrostructure of FZ, **b**, **c** microstructure shows carbide precipitation at top part of weld bead at 50× and 200×, respectively, **d**, **e** microstructure shows carbide precipitation at middle part of weld bead at 100× and 200×, respectively, **f**, **g** microstructure shows carbide precipitation at bottom part of weld bead at 50× and 200×, respectively

Microhardness Properties

Figure 4a, b shows the microhardness variations across and along different zones of the weld. Figure 4a shows the microhardness along the weld bead, and the microhardness in the as-welded conditions increased from top (192.3 VHN) to bottom (226.8 VHN) of the weld. The reason behind this could be the finer grain structure at the bottom of the weld as compared to top and middle as reported by [20]. On the contrary, the microhardness values decreased after the aging treatment (750 °C for 24 h) by approximately 11% throughout the weld bead. This is due to the precipitation of secondary phases along the grain boundaries. While measuring the microhardness

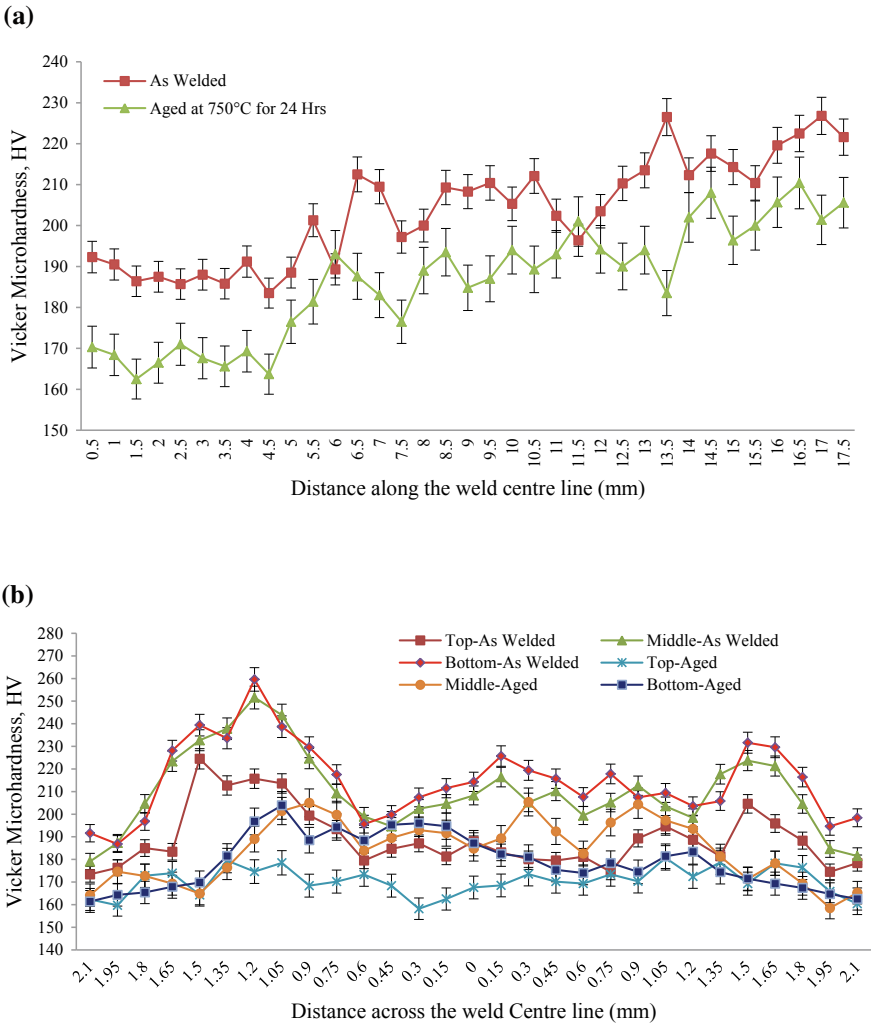

Fig. 4 Vickers microhardness. **a** Along the weld centerline and **b** across the weld centerline

across the weld bead (Fig. 4b), the maximum microhardness obtained was 259.6 VHN at the bottom near the fusion line region in as-welded condition. This could be due to the presence of finer grain structure. The minimum microhardness reported was 158.2 VHN at the top of the weld bead on the parting line after thermal aging. The percentage error in as-welded specimens was 4%, whereas after aging the error increases to 6%. This may be attributed to the formation of precipitates.

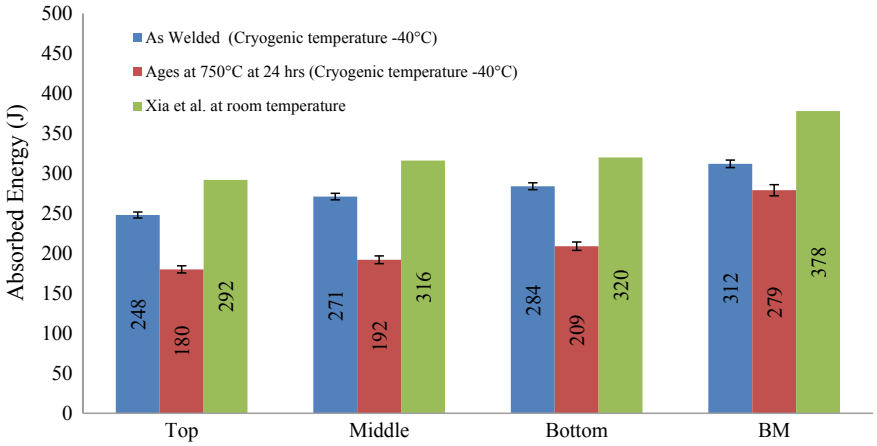

Fig. 5 Impact toughness tested at cryogenic temperature (−40 °C) in as-welded and after aging at 750 °C for 24 h

Impact Toughness Properties

The results of impact test at cryogenic temperature (−40 °C) are presented in Fig. 5. The maximum impact energy of 312 J was absorbed by the base metal in the as-welded condition. It was followed by the impact specimens extracted from bottom and middle of the weld bead in the as-welded condition with average values equal to 284 J and 271 J, respectively. The similar pattern was depicted by Xia et al. [11] while testing at the room temperature. The aging treatment reduced the impact toughness of all the specimens as compared to as-welded specimens. Singh and Shahi [20] observed the same pattern. The percentage error in as-welded specimens was 3%, whereas after aging the error increases to 5%.

Conclusions

The present work reported about the metallurgical and impact toughness of EBW joints of 18-mm-thick AISI 316 SS in as-welded and aged (750 °C for 24 h) condition. The following conclusions could be drawn based on the results.

1. Single-pass, fully penetrated EB welds, with full sidewall fusion, were achieved in 18-mm-thick AISI 316 SS plates with heat input of 1.28 kJ/mm.
2. The weld zone near the fusion boundary of the weld joint had relatively higher microhardness. The aging treatment reduced the microhardness by approximately 11%.

3. The impact toughness of the specimens extracted from the bottom of the weld bead is highest in as-welded condition. However, the base metal had the maximum impact toughness.
4. The aging treatment reduced the impact toughness approximately by 26% due to the precipitation of carbides at the grain boundaries.

Acknowledgements The authors wish to acknowledge the experimental support/facilities extended by the Welding Metallurgy Laboratory, Mechanical Engineering Department, Sant Longowal Institute of Engineering and Technology, Longowal, Sangrur (Deemed University), Punjab, India.

References

1. Karthik V et al (2013) Characterization of mechanical properties and microstructure of highly irradiated SS 316. J Nucl Mater 439(1–3):224–231
2. Raghunathan VS, Seetharaman V, Venkadesan S, Rodriguez P (1979) The influence of post weld heat treatments on the structure, composition and the amount of ferrite in type 316 stainless steel welds. 10(November):1683–1689
3. Kar J, Roy SK, Roy GG (2016) Effect of beam oscillation on electron beam welding of copper with AISI-304 stainless steel. J Mater Process Technol
4. Dutt BS, Sasikala G, Shanthi G, Venugopal S, Babu MN (2011) Mechanical behaviour of SS 316 (N) weld after long term exposure to service temperatures. 0–5
5. Xia X, Wu J, Liu Z, Shen X, Ma J, Liu Z (2019) Study of microstructure difference properties of electron beam welds with beam oscillation of 50 mm 316 L in CFETR. Fusion Eng Des 138(December 2018):339–346
6. Alali M, Todd I, Wynne BP (2017) Through-thickness microstructure and mechanical properties of electron beam welded 20 mm thick AISI 316 L austenitic stainless steel. Mater Des
7. Zumelzu E, Sepu J (1999) Influence of microstructure on the mechanical behaviour of welded 316 L SS joints. 94:36–40
8. Joseph B, Katherasan D, Sathiya P, Murthy CVS (2012) Weld metal characterization of 316 L (N) austenitic stainless steel by electron beam welding process. 4(2):169–176
9. Kim HS et al (2019) Effects of heat treatment on mechanical properties and sensitization behavior of materials in dissimilar metal weld. Int J Press Vessel Pip 172(March):17–27
10. Kozuh S, Gojic M, Kose L (2009) Mechanical properties and microstructure of austenitic stainless steel after welding and post-weld heat treatment. Kov Mater 47(4):253–262
11. Xia X et al. (2019) Correlation between microstructure evolution and mechanical properties of 50 mm 316 L electron beam welds. Fusion Eng Des 147(June):111245
12. Balaji C, Kumar SVA, Kumar SA, Sathish R, Nadu T (2012) Evaluation of mechanical properties of SS 316 L weldments using tungsten inert gas welding. 4(5):2053–2057
13. Kar J, Roy SK, Roy GG (2017) Effect of beam oscillation on microstructure and mechanical properties of AISI 316 L electron beam welds. Metall Mater Trans A Phys Metall Mater Sci 48(4):1759–1770
14. Tjong SC, Zhu SM, Ho NJ, Ku JS (1995) Microstructural characteristics and creep rupture behavior of electron beam and laser welded AISI 316L stainless steel. 227:24–31
15. Shaikh H, Khatak HS, Seshadri SK, Gnanamoorthy JB, Rodriguez P (1995) Effect of ferrite transformation on the tensile and stress corrosion properties of type 316 L stainless steel weld metal thermally aged at 873 K. Metall Mater Trans A 26(7):1859–1868
16. Chen SY, Gan D (1988) Effects of grain boundary carbides on the tensile and impact properties of type 316 stainless steel. Mater Sci Eng 102(2):193–199

17. Zhang M, Chen G, Zhou Y, Liao S (2014) Optimization of deep penetration laser welding of thick stainless steel with a 10 kW fiber laser. Mater Des 53:568–576
18. Elmer JW, Allen SM, Eagar TW (1989) Microstructural development during solidification of stainless steel alloys. Metall Trans A 20(10):2117–2131
19. Brooks JA, Thompsom AW Microstructural development and solidification cracking susceptibility of austenitic stainless steel welds (1)
20. Singh J, Shahi AS (2019) Metallurgical, impact and fatigue performance of electron beam welded duplex stainless steel joints. J Mater Process Technol 272(May):137–148